

Lanthanides in granulometric fractions of Mediterranean soils. Can they be used as fingerprints of provenance?

J. M. MARTÍN-GARCÍA^a , A. MOLINERO-GARCÍA^a, J. CALERO^b ,
M. V. FERNÁNDEZ-GONZÁLEZ^a, J. PÁRRAGA^a & R. DELGADO^a

^aDepartamento de Edafología y Química Agrícola, Universidad de Granada, Campus Cartuja, 18071, Granada, Spain, and ^bDepartamento de Geología, Universidad de Jaén, Campus Las Lagunillas, 23071, Jaén, Spain

Summary

There is geochemical interest in the lanthanides because they behave like a group that is closely related to the parent materials during surface processes, although they also undergo fractionation as a result of supergene dynamics. We analysed lanthanide concentrations (ICPms) in the granulometric fractions fine sand, clay and free forms of clay (FF_{clay-CDB} and FF_{clay-Ox}: extracted with citrate-dithionite-sodium bicarbonate and with ammonium oxalate, respectively) from a soil chronosequence of Mediterranean soils. There was a relative enrichment of heavy rare earth elements (HREE) in the clay fraction and its free forms with respect to fine sand. The clay free forms behaved as scavengers of lanthanides, and oxidative scavenging of cerium (Ce) in FF_{clay-CDB} was also detected. Lanthanide concentrations (lanthanum to gadolinium in fine sand; terbium to lutetium in clay) varied with soil age, and chronofunctions were established. There was a strong positive collinearity between most of the lanthanide concentrations. Furthermore, the value of the correlation index (Pearson's *r*) of the concentrations between couples of lanthanides (r_{CLC}) decreased significantly with increasing separation between the elements in the periodic table; this has never been described in soils. Several geochemical properties and indices in the fine sand and clay soil fractions and in the geological materials of the Guadalquivir catchment showed, on the one hand, a genetic relation between them all, enabling the lanthanides to be used as fingerprints of provenance; on the other hand, fractionation between fine sand and clay showed these are actively involved in soil lanthanide dynamics.

Highlights

- Are lanthanides from fine sand and clay genetically related to the geological materials?
- Lanthanide concentrations of fine sand and clay fit chronofunctions
- Pearson's *r* of lanthanide couples decreases when separation increases in the periodic table
- Free forms of clay are scavengers of lanthanides and concentrate HREE and cerium

Introduction

Quantities of rare earth elements (REE) (lanthanoids: $_{57-71}\text{Ln}$, and scandium $_{21}\text{Sc}$ and yttrium $_{39}\text{Y}$) in the Earth's crust are of the order mg kg^{-1} , and show some characteristic periodic behaviour such as: (i) light REE (LREE), low atomic weight (A_r) (lanthanum La to samarium Sm), are more abundant than heavy REE (HREE) (holmium Ho to lutetium Lu) (British Geological Survey, 2011) (medium REE, MREE: samarium Sm to dysprosium Dy, have an intermediate A_r ; Rollinson, 1993) and (ii) a strong linear correlation

between their concentrations has been reported; in European soils, $r > 0.7$ (Salminen, 2005).

The chemical signatures of the parent rock assemblages in a tectonic province can persist in the daughter sediments produced, and are thus preserved in the corresponding sedimentary deposits (Rollinson, 1993). It has been suggested (Blundy & Wood, 2003) that the trace elements (<0.1% by weight, as in the case of lanthanides) exhibit passive behaviour during supergene processes, resulting in their being excellent tracers of the source area of sediments and soil materials. Wang *et al.* (2017) described them as ideal tracers of origin in aeolian research. Consequently, the geochemical interest in the lanthanides is because of their close relation

Correspondence: R. Delgado. E-mail: rdelgado@ugr.es

Received 26 February 2018; revised version accepted 11 July 2018

with the source area. This feature can be used in paleoenvironmental studies of sedimentary origin and tectonic setting (Chen *et al.*, 2014; Och *et al.*, 2014), and in soil studies such as pedogenic tracers (Laveuf & Cornu, 2009). The concentrations of REE in soil have been shown to depend not only on the lithology over which they develop, but also there are soil processes that induce internal fractionation or anomalies (Laveuf & Cornu, 2009). The Ln patterns, where the abundance of each Ln relative to that of a chondrite or shale is plotted on a logarithmic scale against the atomic number, or the geochemical ratios between lanthanides (e.g. HREE/LREE, lanthanum/ytterbium (La/Yb), samarium/ytterbium (Sm/Yb), and so on, or the cerium and europium anomalies (Ce/Ce* and Eu/Eu*, respectively)) are used for studying the provenance of geological materials (as fingerprints) and for analysing pedogenic intensity (Rollinson, 1993; Moreno *et al.*, 2006; Mongelli *et al.*, 2014). In soil lanthanide dynamics, another process to add to inheritance and pedogenic action is aeolian contribution. Aeolian processes are common in Mediterranean soils (Delgado *et al.*, 2003).

Relatively little is known about lanthanide behaviour in soil (Chen *et al.*, 2014); therefore, their dynamics in different soil environments need to be analysed (Laveuf *et al.*, 2012). Studies of REE concentrations of granulometric fractions of soils, including sands (2000–50 µm) (Aide & Smith-Aide, 2003; Marques *et al.*, 2011) or in free forms, or in soil chronosequences are even more scarce (Chang *et al.*, 2016; Martín-García *et al.*, 2016).

The aim of the present study was to examine lanthanide concentrations in the fine sand and clay fractions and the free forms of clay from a soil chronosequence from the River Guadalquivir (southern Spain) (a soil chronosequence is a series of soils that differ in their degree of profile development because of differences in age, while other soil-forming factors remain relatively constant). Other novel aspects investigated in this study are: (i) the effect of soil age, including the formulation of chronofunctions, (ii) the correlations between concentrations, (iii) the use of lanthanides as fingerprints of provenance compared with geological samples from the same soil zone and (iv) the contribution to the soil of lanthanides from aeolian materials.

In previous studies we have shown how the soils of the Guadalquivir behave like an ideal chronosequence, in which a considerable number of components and properties fitted significantly to chronofunction equations (Calero *et al.*, 2008, 2009, 2013). In addition, Martín-García *et al.* (2016) have studied the geochemistry of the clay fraction (including some aspects of lanthanides).

The present study can be included in the collection of soil chronofunction studies, which, at present, are few.

Materials and methods

Setting and soils

Geographically, the Guadalquivir River (640-km long) drains an area of 68 300 km². It rises in the Baetic Cordillera at a height of 1400 m before flowing into the Atlantic Ocean. It is the most important fluvial system in the southern Iberian Peninsula. From

a geological point of view, the Guadalquivir-Cenozoic Basin was developed between the Iberian Massif (passive margin) to the north and the Baetic Cordillera (active margin) to the south (Figure 1). From a sedimentological point of view their fluvial alluvia are gravels with some stone-free sandy silt layers. The source rocks for this alluvium are lithologically diverse and include: to the north, igneous rocks (such as granite, granodiorite, rhyolite, tonalite, andesite, gabbro and intrusive rocks) and metamorphic rocks (mainly shales) from the Iberian Massif (Central Iberian Zone, mainly *Los Pedroches* batholith and *Santa Elena* pluton, and the Iberian Massif) (Larrea *et al.*, 1992, 1994, 1995; Carracedo *et al.*, 1997; Pin *et al.*, 2002; Pascual *et al.*, 2008); to the south and west, sedimentary materials such as limestones, marly limestones, marls and dolomites from the External Baetics Zone of the Baetic Cordillera (Martínez-Ruiz, 1994), metasedimentary rocks (schist and gneiss) from the Internal Baetics Zone (Torres-Ruiz *et al.*, 2003) and Quaternary sediments from the Guadalquivir Depression, a Cenozoic Basin (Jiménez-Espinosa *et al.*, 2016).

The study area is in the middle reaches of the Guadalquivir River, near the town of Andújar on a transect of 3.7 km along the river between 3°50′–4°3′W and 38°0′–38°2′N (Figure 1). The soils selected (Table 1) developed on four Quaternary terrace surfaces (P1, P2, P3 and P4: Luvisols and Calcisols) and a floodplain (P5: Fluvisol) with ages ranging from 600 to 0.3 ka (Calero *et al.*, 2008). Fresh point bar sediments (PM) in the river were also selected. Currently, the climate is hot in the Mediterranean with mean annual rainfall of 650 mm and a mean annual temperature of 18 °C. The vegetation is mainly anthropogenic because the flat surfaces have been cultivated since time immemorial (nowadays olive groves, wheat and cotton).

The solum of the older terrace soils (pre-Holocene soils: P1, P2 and P3) (Table 1) shows Bt horizons (with clay illuviation features such as clay cutans), red Munsell colours, relatively deep thickness, clayey textures (> 30% clay) and evidence of leaching of carbonates (and accumulation, in P2). Thus, the older soils have the largest values of Harden's profile development index (between 44.8 for P1 and 39.6 for P3; Table 1). In the Holocene soil P4, brunification and some leaching and accumulation of carbonates has also been detected. The soil P5 had no evident evolution features. In the fine sand fraction (Table 1), quartz was the main mineralogical component in P1, P2 and P3 (≥ 58%, mean value), whereas the carbonates, calcite and dolomite were the main components in P4 and P5 (≥ 44%, mean value of total carbonates). Other phases present were phyllosilicates (illite, brammallite, chlorite, kaolinite and various mixed-layer phases), feldspars (potassium feldspar and plagioclases, both abundant in P3) and iron (hydr)oxides (goethite and haematite). The point bar sediment PM showed a more balanced composition of quartz and carbonates (30 and 40%, respectively).

Materials and lanthanide analyses

Lanthanide concentrations of the fine sand fraction (50–250 µm) of 24 samples (belonging to soil horizons and point bar sediment, PM) were determined by inductively coupled plasma–mass

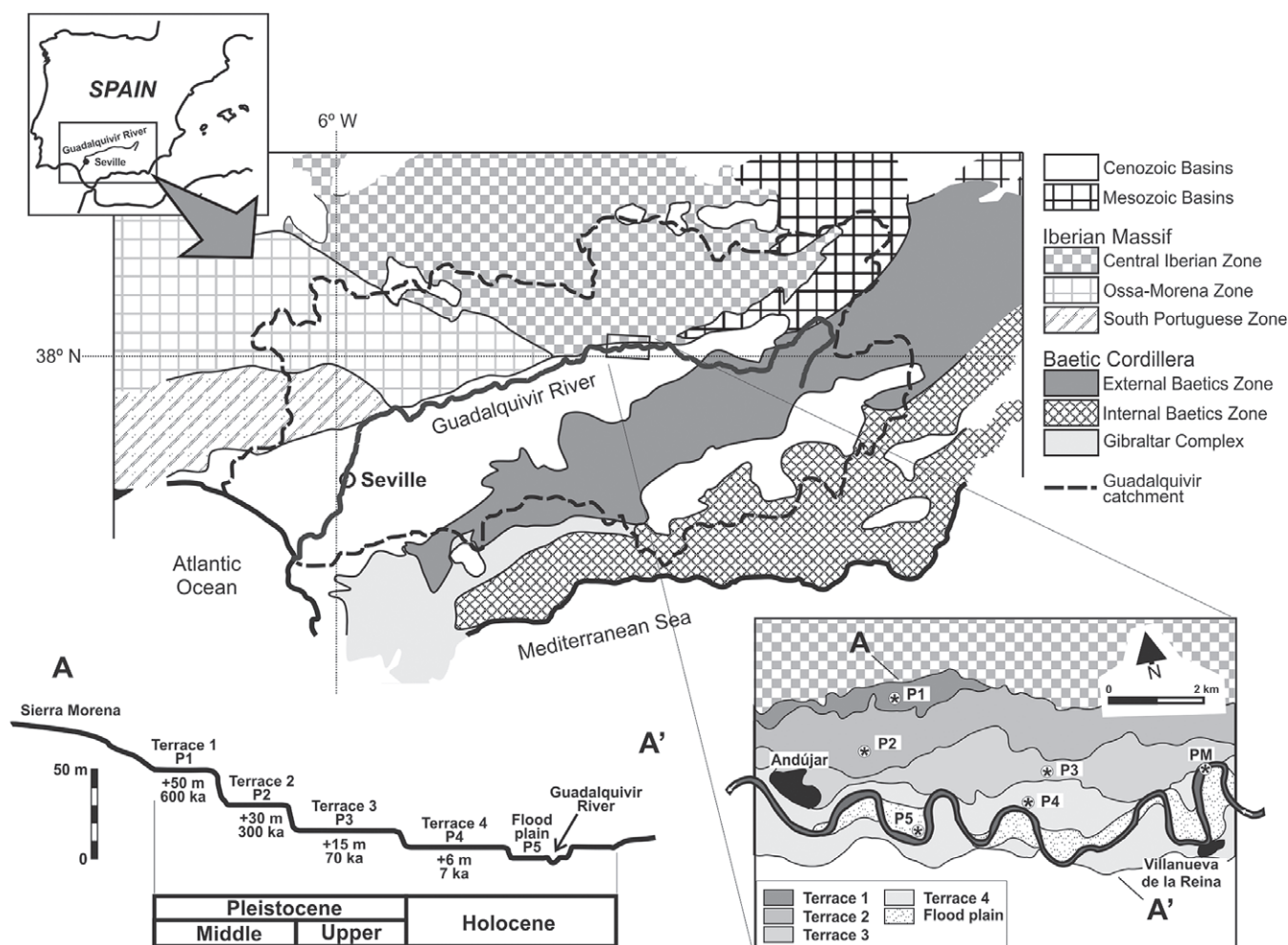


Figure 1 Location of the study area, geology of the Guadalquivir catchment, position of fluvial terrace levels (Terraces 1 to 4 and flood plain), topographic profile (A–A') and soil sampling (P1 to P5 and PM).

spectrometry (ICP–MS) using an Agilent 7700x (Santa Clara, CA, USA) instrument at the Natural History Museum (London, UK) after lithium metaborate fusion in a Pt–Au crucible, and the resulting flux was dissolved in 10% HNO₃. Calibration was performed using certified reference materials (CRM) prepared in the same way. Further analytical details are given in Gregory *et al.* (2017). As study material, we also used the concentrations of lanthanides from the clay fraction and the free forms of clay after extraction with citrate-dithionite-bicarbonate (FF_{clay-CDB}) or with ammonium oxalate (FF_{clay-Ox}), measured previously by Martín-García *et al.* (2016). The FF_{clay-CDB} is conventionally assumed to be a measure of the total pedogenic free forms (crystalline and poorly crystalline forms), whereas FF_{clay-Ox} is a measure of poorly crystalline forms; mainly iron, but with appreciable quantities of Al and Ti.

We grouped lanthanides following Rollinson (1993) into light (LREE: La to Nd), medium (MREE: Sm to Dy) and heavy rare earth elements (HREE: Ho to Lu). Lanthanide concentrations were normalized to (i.e. divided by) the CI chondrite, considered to represent the bulk earth composition, of McDonough & Sun

(1995), and then the Ce/Ce* and Eu/Eu* anomalies were calculated ($Ce/Ce^* = Ce_N / (La_N \times Pr_N)^{1/2}$; $Eu/Eu^* = Eu_N / (Sm_N \times Gd_N)^{1/2}$; the subscript _N shows that the value was normalized by the chondrite used. It makes sense to calculate both anomalies because Eu³⁺ and Ce³⁺ might be in another valency (Eu²⁺ and Ce⁴⁺) and thus be involved in different reactions from those of the rest of the trivalent lanthanides (Ln³⁺) (i.e. separate from the group behaviour). The ratios La_N/Yb_N , Sm_N/Yb_N , $HREE_N/LREE_N$ and $MREE_N/LREE_N$ were also calculated; all establish the degree of fractionation of LREE from MREE and HREE (La is a representative of LREE, Sm of MREE and Yb of HREE) during geochemical processes.

Statistical analysis

The statistical analysis was carried out using the IBM SPSS v.22.0 software package. The Kolmogorov–Smirnov and Shapiro–Wilk tests were used to determine the normality of data, and the results were considered statistically significant if *P* was less than 0.05. Statistical analyses were carried out after data were transformed

Table 1 Soil characteristics^a. Mean values and standard deviation (in parentheses)

Profile (Terrace No)	Soil classification ^b	Age/ ka	Fine earth fraction (< 2 mm)					Mineralogy (XRD) / %														
			PDI	Clay / %	Fine sand / %	OC / %	pH	CEC / cmol _c kg ⁻¹	FF _{CDB} / %	CaCO ₃ eq / %	FF _{day-CDB} / %	FF _{day-Ox} / %	Fine sand (50–250 µm)					Clay (< 2 µm)				
													phy	qz	fd	feox	ca	do	phy	qz	fd	feox
P1 (Terrace 1)	Cutanic Luvisol/ Palexeralf	600 ^c	44.8 (7.2)	29.4 (9.6)	35.8 (9.6)	0.24 (0.14)	7.4 (0.4)	8.5 (1.8)	3.64 (0.44)	0.5 (0.9)	5.61 (0.83)	0.38 (0.06)	29 (9)	61 (10)	6 (3)	3 (1)	1 (0)	86 (1)	8 (1)	1 (1)	5 (1)	0 (0)
P2 (Terrace 2)	Lixic Cal- cisol/ Haploxeralf	300 ^c	44.3 (5.5)	42.9 (13.4)	21.4 (13.4)	0.32 (0.23)	7.9 (0.1)	15.1 (2.8)	3.24 (0.36)	16.9 (19.4)	3.66 (0.35)	0.38 (0.06)	18 (6)	58 (8)	12 (10)	3 (1)	9 (10)	87 (1)	5 (1)	2 (1)	4 (1)	2 (1)
P3 (Terrace 3)	Cutanic Luvisol/ Haploxeralf	70 ^c	39.6 (7.5)	30.7 (9.2)	36.4 (9.2)	0.22 (0.09)	7.6 (0.2)	10.7 (7.7)	1.90 (0.34)	0 (0.0)	3.06 (0.28)	0.53 (0.10)	6 (2)	58 (10)	31 (10)	2 (1)	3 (3)	89 (2)	6 (1)	2 (1)	3 (1)	0 (1)
P4 (Terrace 4)	Haplic Calcisol/ Calcixerapt	7 ^d	26.8 (8.5)	24.5 (6.8)	29.9 (6.8)	0.37 (0.25)	8.2 (0.4)	8.9 (6.1)	1.80 (0.48)	24.2 (7.1)	1.60 (0.43)	0.33 (0.05)	14 (5)	30 (15)	9 (7)	3 (1)	14 (5)	87 (3)	3 (1)	2 (1)	2 (1)	6 (3)
P5 Flood plain	Haplic Fluvisol/ Xerofluvent	0.3 ^d	21.2 (3.4)	17.5 (8.2)	43.0 (8.2)	0.41 (0.19)	8.0 (0.1)	6.9 (3.3)	1.27 (0.11)	39.0 (1.9)	1.15 (0.15)	0.45 (0.11)	20 (8)	26 (5)	6 (3)	2 (1)	29 (3)	88 (1)	3 (2)	1 (0)	1 (1)	7 (0)
PM ^e			0	16.3	21.6	1.76	8.4	8.7	0.78	23.5	1.06	0.60	17	30	10	3	33	85	3	2	1	9

^aFrom Calero *et al.* (2009) and Martín-García *et al.* (2016).^bWorld Reference Base for Soil Resources/Soil Taxonomy.^cPre-Holocene.^dHolocene.^eParent material: Fluvial sediment 'point bar'.PDI, profile development index (Harden, 1982); OC, organic carbon; CEC, cation exchange capacity; FF_{CDB}, citrate-dithionite-bicarbonate extractable free forms in the fine earth fraction (Fe₂O₃ + Al₂O₃); FF_{day-CDB}, citrate-dithionite-bicarbonate extractable free forms in the clay fraction (Fe₂O₃ + Al₂O₃ + TiO₂); FF_{day-Ox}, ammonium oxalate extractable free forms in the clay fraction (Fe₂O₃ + Al₂O₃ + TiO₂); CaCO₃ eq, calcium carbonate equivalent; phy, phyllosilicates (illite, smectite, mixed-layer phases, kaolinite, chlorite, brammallite); qz, quartz; fd, feldspar; feox, iron (hydr)oxides (goethite, hematite); ca, calcite; do, dolomite.

logarithmically if this was necessary. The matrix of Pearson's product-moment correlation coefficients (r) and, in some cases, the coefficients of determination (R^2) were obtained. The coefficient of determination (R^2) was obtained to determine the fit of the least squares regressions.

Results and discussion

Lanthanides in the fine sand fraction

The series of lanthanides in fine sand showed very variable values, ranging from around 0.05 to 65 mg kg⁻¹ (Table 2). The order of abundance was Ce > La > Nd > Pr > Sm > Gd > Dy > Er > Yb > Eu > Ho > Tb > Tm > Lu, identical to that of the mean of the Earth's crust (Rollinson, 1993; British Geological Survey, 2011), so that $\Sigma\text{LREE} > \Sigma\text{MREE} > \Sigma\text{HREE}$ (Table 3). Lanthanide concentration increased with depth in the profile (Table 2). The P1 horizons contained most ΣLn (Table 3). The ΣLREE increased with age (P1 > P2 > P3 > P4 > P5 > PM) and profile P4 was the richest in ΣHREE and Dy (e.g. horizon 4C2 had the largest concentration). The ratios $\text{MREE}_\text{N}/\text{LREE}_\text{N}$ and $\text{HREE}_\text{N}/\text{LREE}_\text{N}$ were smaller in pre-Holocene than Holocene soils and PM (Table 3).

The concentrations of lanthanides (ΣLn) were related to those of phyllosilicates, as proposed by Mongelli *et al.* (2014). In the fine sand of the present study, this is determined as:

$$\Sigma\text{Ln} \text{ (mg kg}^{-1}\text{)} = 1.85 \times \text{Phyllosilicates (\%)} + 59.08 \text{ (} n = 24; r = 0.538; P < 0.01\text{)}.$$

In addition, the abnormally large concentrations of Dy and HREE in 4C2 of profile P4 (Table 2) reaffirm the presence of the lithological discontinuity detected morphologically by Calero *et al.* (2008, 2009). A possible explanation might be a change in the mineralogical composition of the major species (phyllosilicates, quartz, feldspars, iron oxides, calcite and dolomite) compared with the other horizons of the profile. However, this mineralogical change was not detected (table 4 on page 471 of Calero *et al.*, 2009). Therefore, it must be assumed that the change is in the minority mineral phases (< 1%), which are those having an important role in lanthanide concentration (Kerr & Rafuse, 2012). Thus, the excess of Dy and HREE in geologic materials might be a result of the presence of minerals such as thortveitite, with the formula (Sc,Y)Si₂O₇, which can show detectable concentrations of Dy, Ho, Er, Tm, Yb and Lu (Guastoni *et al.*, 2012), or xenotime, with the formula (HREE,Y)PO₄. However, verification of this would be beyond the scope of the present study.

The chondrite-normalized profiles (Figure 2a) always had values > 1 (i.e. larger quantities than in the reference meteorite), a common tendency in soil materials (Hu *et al.*, 2006). Figure 2(a) also indicates a pronounced relative abundance of LREE, shown by a steep slope that flattens out in such a way that after Ho (region of the HREE) it is almost horizontal. The P1 horizons, with more lanthanides, occupy the highest positions on the graph and the

4C2 horizon of P4 is V-shaped because of its large Dy and HREE concentrations.

No notable Ce/Ce* anomaly was detectable (Figure 2a, Table 3), with values very close to unity (all horizons between 0.93 and 1.04). The mean values of Ce/Ce* per profile increased with soil age, probably as a result of alteration processes in the soil material (Huang & Gong, 2001). In the present study, the alteration could be related to decarbonation of the fine sand (decrease in calcite and dolomite content through leaching) (Table 1), as shown by the moderate negative correlation in fine sand between Ce/Ce* and the sum of calcite + dolomite, % ($r = -0.530$, $n = 22$, $P < 0.01$), which accords with the results of Wen *et al.* (2014), in their case with $r = -0.403$ and $P < 0.01$.

According to its lanthanides, the fine sand fraction has evolved geochemically rather than being inert.

Lanthanides in the clay fraction and clay free forms

In the clay fraction, the order of abundance of ΣLn (mean values per profile in mg kg⁻¹) is: P3 > P2 > P4 > P1 > P5 > PM (Table 3), with no obvious trend regarding age or when compared with the respective fine sand (Table 3). Aide & Smith-Aide (2003) and Marques *et al.* (2011) reported that the lanthanides are concentrated in the fine fractions, < 50 μm (silt and clay); in the present study, this was not clear in P1 and P5. This might be a result of the differences in phyllosilicate content because these were always larger in the clay (Table 1), and in P1 and P5 this would suggest searching for the presence of lanthanide-rich minerals (e.g. zircon) in fine sand; again, this is beyond the scope of the present study. Moreover, in the clay fraction, as occurred in the fine sand, there was a relation between ΣLn and phyllosilicates ($n = 35$, $r = 0.566$, $P < 0.001$). Considering the complete population (clay + fine sand), this correlation was not significant.

The clay of the pre-Holocene soils (P1, P2 and P3) contained more ΣHREE than that of two of the Holocene soils (P4 and P5) and PM. Furthermore, the clay of these pre-Holocene soils also had more ΣHREE than the corresponding fine sand (Table 3).

The clay free forms ($\text{FF}_{\text{clay-CDB}}$ and $\text{FF}_{\text{clay-Ox}}$) generally contained fewer lanthanides (ΣLn) than the fine sand and clay fractions (Table 3). However, calculation of ΣLn in $\text{FF}_{\text{clay-CDB}}$, assuming that all proceed from the mineral phases that constitute the free forms (in $\text{FF}_{\text{clay-CDB}}$ it was mainly goethite, haematite and poorly crystalline forms of Fe; in $\text{FF}_{\text{clay-Ox}}$ it was poorly crystalline iron, mostly ferrihydrite; Martín-García *et al.*, 2016), provided striking new evidence of REE accumulation in iron free forms. Thus, $\text{FF}_{\text{clay-CDB}}$ of P1, with ΣLn of 39.82 mg kg⁻¹ attributable to 5.61% of $\text{FF}_{\text{clay-CDB}}$ ($\text{Fe}_2\text{O}_3 + \text{Al}_2\text{O}_3 + \text{TiO}_2$; Table 1), suggests that iron (hydr)oxides ($\text{FF}_{\text{clay-CDB}}$) had ΣLn of 709.8 mg kg⁻¹. When the calculation was carried out with PM (1.06% $\text{FF}_{\text{clay-CDB}}$ ($\text{Fe}_2\text{O}_3 + \text{Al}_2\text{O}_3 + \text{TiO}_2$; Table 1) and 9.60 mg kg⁻¹ of ΣLn) the goethite + haematite had 905.7 mg kg⁻¹. These values of ΣLn can be attributed to the special characteristics of these iron (hydr)oxides: small particle size and neoformed in the soil, absorbing Ln at their surface, which might even have been buried during the growth of the iron (hydr)oxide.

Table 2 Lanthanide content (mg kg^{-1}) in the soil fine sand fraction (50–250 μm)

	La	Ce	Pr	Nd	Sm	Eu	Gd	Tb	Dy	Ho	Er	Tm	Yb	Lu
P1 Ap	24.93	53.69	6.37	23.03	4.14	0.66	2.92	0.35	1.87	0.32	0.97	0.14	0.93	0.15
Bt	29.55	64.30	7.58	28.09	5.29	0.93	4.03	0.52	2.97	0.51	1.49	0.21	1.50	0.22
Btg2	31.78	66.50	7.97	29.82	5.66	1.05	4.22	0.53	3.05	0.53	1.56	0.23	1.56	0.22
2BCtg	26.21	54.91	6.69	25.06	4.91	0.95	3.51	0.42	2.37	0.40	1.29	0.17	1.29	0.19
4C	29.86	61.30	7.32	26.78	5.11	0.93	3.54	0.44	2.46	0.41	1.23	0.18	1.27	0.19
Mean ^a	28.85 (2.81)	60.92 (5.66)	7.29 (0.65)	27.02 (2.63)	5.14 (0.57)	0.94 (0.15)	3.75 (0.51)	0.47 (0.07)	2.64 (0.48)	0.45 (0.09)	1.36 (0.23)	0.19 (0.04)	1.37 (0.25)	0.20 (0.03)
P2 Ap	10.79	21.59	2.51	9.08	1.66	0.34	1.13	0.14	0.8	0.15	0.42	0.06	0.45	0.07
Btg1	18.82	37.44	4.66	17.06	3.18	0.64	2.53	0.34	1.95	0.38	1.05	0.15	0.99	0.15
Btg2	17.09	32.75	3.73	13.26	2.35	0.50	1.67	0.21	1.23	0.23	0.67	0.11	0.68	0.10
Cmk/Bt	23.76	48.96	6.04	22.56	4.28	0.80	3.20	0.40	2.25	0.46	1.19	0.17	1.09	0.18
Mean ^a	17.66 (5.36)	35.20 (11.34)	4.20 (1.49)	15.35 (5.73)	2.83 (1.13)	0.56 (0.20)	2.08 (0.92)	0.26 (0.12)	1.51 (0.66)	0.29 (0.14)	0.80 (0.35)	0.12 (0.05)	0.78 (0.29)	0.12 (0.05)
P3 Ap1	11.97	22.72	2.96	10.72	2.06	0.37	1.47	0.19	1.12	0.21	0.63	0.09	0.59	0.09
Bt1	17.30	32.51	4.16	15.06	2.95	0.45	1.99	0.27	1.56	0.30	0.94	0.13	0.83	0.13
Bt2	15.00	28.97	3.65	12.75	2.46	0.42	1.77	0.23	1.33	0.25	0.77	0.11	0.71	0.11
Bt3	18.86	38.83	4.75	17.31	3.37	0.47	2.43	0.31	1.83	0.36	1.09	0.15	0.92	0.14
Bt4	17.50	35.79	4.26	15.35	2.87	0.50	2.01	0.27	1.46	0.28	0.82	0.12	0.74	0.11
2Bt6	23.32	47.41	5.69	20.24	3.86	0.51	2.94	0.44	2.70	0.53	1.54	0.23	1.41	0.22
Mean ^a	18.01 (3.81)	35.78 (8.49)	4.41 (0.93)	15.85 (3.35)	3.05 (0.64)	0.46 (0.05)	2.19 (0.52)	0.30 (0.09)	1.76 (0.56)	0.34 (0.11)	1.02 (0.32)	0.15 (0.05)	0.91 (0.29)	0.14 (0.05)
P4 Ap1	11.21	21.74	2.80	10.43	2.10	0.45	1.63	0.22	1.34	0.26	0.78	0.11	0.65	0.10
Bwk1	12.53	24.01	3.06	11.32	2.23	0.47	1.76	0.24	1.47	0.29	0.84	0.12	0.71	0.11
2Bwk2	26.43	54.91	6.47	23.59	4.38	0.54	3.02	0.37	2.11	0.38	1.17	0.19	1.11	0.17
4C2	13.33	26.26	3.26	12.25	2.52	0.54	2.76	0.54	4.41	1.01	3.50	0.53	3.45	0.54
Mean ^a	16.80 (7.09)	33.77 (15.56)	4.12 (1.73)	15.21 (6.17)	2.96 (1.06)	0.51 (0.05)	2.48 (0.70)	0.38 (0.15)	2.71 (1.43)	0.57 (0.35)	1.89 (1.30)	0.29 (0.20)	1.81 (1.33)	0.28 (0.21)
P5 Ap	16.03	31.08	4.02	15.25	3.03	0.61	2.57	0.34	2.09	0.38	1.13	0.15	0.94	0.17
2C1	12.51	24.40	3.13	11.98	2.38	0.51	1.96	0.26	1.70	0.32	0.97	0.13	0.81	0.12
4C3	16.78	34.21	4.07	15.26	2.99	0.58	2.54	0.34	2.03	0.39	1.17	0.16	1.03	0.16
6C5	15.39	29.65	3.74	13.95	2.72	0.53	2.40	0.33	2.04	0.39	1.16	0.16	1.01	0.15
Mean ^a	15.09 (1.87)	29.72 (4.09)	3.73 (0.43)	14.09 (1.55)	2.78 (0.30)	0.56 (0.05)	2.36 (0.28)	0.31 (0.04)	1.95 (0.18)	0.37 (0.03)	1.10 (0.09)	0.15 (0.01)	0.94 (0.10)	0.15 (0.02)
PM	10.41	19.98	2.58	9.76	2.01	0.43	1.56	0.20	1.23	0.24	0.72	0.10	0.61	0.09

^aWeighted to horizon thickness (standard deviation in parentheses).

Table 3 Total content and selected geochemical ratios of lanthanides. Mean profile values and standard deviation (in parentheses). Soil fine sand and soil clay fractions and free forms of the soil clay fraction extracted with citrate-dithionite-bicarbonate (FF_{clay-CDB}) and oxalate (FF_{clay-Ox}).

	$\Sigma\text{Ln}/\text{mg kg}^{-1}$	$\Sigma\text{LREE}/\text{mg kg}^{-1}$	$\Sigma\text{MREE}/\text{mg kg}^{-1}$	$\Sigma\text{HREE}/\text{mg kg}^{-1}$	$\text{MREE}_\text{N}/\text{LREE}_\text{N}$	$\text{HREE}_\text{N}/\text{LREE}_\text{N}$	Eu/Eu^*	Ce/Ce^*
Soil fine sand (50–250 μm) ($n = 24$)								
P1	140.59 (12.87)	124.08 (11.65)	12.94 (1.75)	3.57 (0.63)	0.26 (0.02)	0.12 (0.01)	0.65 (0.05)	1.02 (0.02)
P2	81.77 (15.34)	72.40 (23.85)	7.24 (3.01)	2.12 (0.88)	0.25 (0.02)	0.12 (0.02)	0.73 (0.06)	0.99 (0.02)
P3	84.37 (14.15)	74.04 (16.54)	7.76 (1.82)	2.56 (0.82)	0.26 (0.01)	0.14 (0.02)	0.55 (0.07)	0.97 (0.04)
P4	83.80 (35.71)	69.91 (30.55)	9.05 (2.69)	4.85 (3.39)	0.31 (0.10)	0.28 (0.26)	0.61 (0.13)	0.97 (0.04)
P5	73.29 (9.86)	62.63 (7.86)	7.96 (0.83)	2.70 (0.26)	0.31 (0.01)	0.17 (0.01)	0.67 (0.04)	0.96 (0.03)
PM	49.92	42.73	5.43	1.76	0.32	0.16	0.74	0.93
Soil clay (< 2 μm) ($n = 35$)								
P1	86.99 (12.31)	71.75 (10.71)	11.10 (1.25)	4.14 (0.37)	0.39 (0.01)	0.24 (0.02)	0.67 (0.02)	0.94 (0.01)
P2	105.23 (15.80)	90.73 (13.20)	10.50 (2.08)	4.00 (0.53)	0.30 (0.01)	0.19 (0.01)	0.66 (0.01)	1.15 (0.08)
P3	143.01 (26.60)	123.25 (23.61)	14.86 (2.42)	4.90 (0.69)	0.30 (0.01)	0.16 (0.01)	0.65 (0.01)	1.00 (0.05)
P4	97.84 (34.20)	83.67 (29.50)	10.68 (3.67)	3.49 (1.05)	0.32 (0.01)	0.17 (0.01)	0.63 (0.04)	1.04 (0.03)
P5	68.81 (17.10)	58.63 (14.79)	7.58 (1.75)	2.60 (0.56)	0.33 (0.01)	0.18 (0.01)	0.69 (0.01)	0.98 (0.01)
PM	51.46	43.72	5.74	2.00	0.33	0.19	0.71	0.99
FF _{clay-CDB} ($n = 35$)								
P1	39.82 (10.08)	31.07 (8.49)	6.92 (1.33)	1.83 (0.27)	0.58 (0.07)	0.25 (0.04)	0.75 (0.02)	1.09 (0.11)
P2	45.74 (13.45)	38.10 (10.92)	5.87 (2.00)	1.77 (0.54)	0.44 (0.01)	0.21 (0.01)	0.71 (0.03)	1.74 (0.33)
P3	67.41 (12.30)	54.91 (10.20)	9.45 (1.64)	3.05 (0.41)	0.47 (0.04)	0.24 (0.02)	0.71 (0.01)	1.39 (0.07)
P4	13.64 (3.09)	10.83 (2.62)	2.05 (0.36)	0.76 (0.13)	0.53 (0.04)	0.31 (0.02)	0.74 (0.03)	1.50 (0.19)
P5	14.66 (6.03)	11.58 (4.97)	2.29 (0.84)	0.79 (0.23)	0.51 (0.04)	0.29 (0.05)	0.75 (0.04)	1.05 (0.03)
PM	9.60	7.66	1.44	0.50	0.49	0.27	0.75	1.03
FF _{clay-Ox} ($n = 35$)								
P1	1.76 (0.86)	0.92 (0.54)	0.55 (0.22)	0.29 (0.11)	1.39 (0.46)	1.34 (0.43)	0.65 (0.35)	0.86 (0.09)
P2	1.22 (0.84)	0.61 (0.53)	0.36 (0.20)	0.25 (0.11)	1.58 (1.30)	1.91 (2.21)	0.88 (0.36)	1.83 (1.09)
P3	3.93 (1.12)	2.26 (0.74)	0.98 (0.26)	0.69 (0.18)	1.09 (0.20)	1.35 (0.18)	0.55 (0.06)	1.40 (0.36)
P4	1.02 (0.37)	0.66 (0.25)	0.24 (0.10)	0.13 (0.06)	0.83 (0.31)	0.84 (0.58)	0.24 (0.09)	1.24 (0.46)
P5	0.61 (0.23)	0.28 (0.14)	0.17 (0.06)	0.16 (0.05)	1.41 (0.32)	2.35 (1.65)	1.08 (0.43)	0.92 (0.56)
PM	0.58	0.25	0.20	0.13	2.11	2.89	0.34	2.22

Ln, La to Lu; LREE, La to Nd; MREE, Sm to Dy; HREE, Ho to Lu; the suffix “_N” shows that the value normalized to chondrite was used; $\text{Eu}/\text{Eu}^* = \text{Eu}_\text{N}/(\text{Sm}_\text{N} \times \text{Gd}_\text{N})^{1/2}$; $\text{Ce}/\text{Ce}^* = \text{Ce}_\text{N}/(\text{La}_\text{N} \times \text{Pr}_\text{N})^{1/2}$; FF_{clay-CDB}, citrate-dithionite-bicarbonate extractable free forms in clay fraction; FF_{clay-Ox}, ammonium oxalate extractable free forms in clay fraction.

This proves that iron (hydr)oxides act as lanthanide scavengers. Our values were small considering that Onac *et al.* (1997) reported $\Sigma(\text{La}, \text{Ce}, \text{Sm}, \text{Nd})$ greater than 2000 mg kg⁻¹ in coatings of ferromanganese (hydr)oxides.

The ΣLn in the clay free forms (FF_{clay-CDB} and FF_{clay-Ox}) tended to increase with soil age because they were more abundant in pre-Holocene soils than in Holocene soils and PM (Table 3).

The chondrite-normalized patterns (Figure 2b) showed that in most cases the clay was within the range of concentrations of fine sand. The profiles of FF_{clay-CDB} (Figure 2c) differentiate clearly between the pre-Holocene soils (P1, P2, P3) and the Holocene soils (P4, P5) and PM, which had smaller concentrations.

The ratio $\text{HREE}_\text{N}/\text{LREE}_\text{N}$ in the clay fraction (Table 3) was greater than in the fine sand (except in P4). Laveuf & Cornu (2009) stated that during pedogenesis the LREE are less readily complexed by fluids than the HREE and that the latter accumulate in alteration products such as phyllosilicates, which are more abundant in the clays than in the fine sand. Furthermore, the $\text{HREE}_\text{N}/\text{LREE}_\text{N}$ index was greater in FF_{clay-CDB} and FF_{clay-Ox} (neofomed iron (hydr)oxides) than in fine sand or clay, which was in accord

with Pédrot *et al.* (2015), who reported that the iron (hydr)oxides precipitated during alteration have a greater affinity for HREE than for LREE. This all suggests fractionation of the Ln by granulometric fractions (and mineralogy), with the HREE being concentrated in the clay, FF_{clay-CDB} and FF_{clay-Ox}.

The values of the Ce/Ce^* anomaly of the clay fraction (0.94–1.14) (Table 3, Figure 2a) were also similar to those of the fine sand. In FF_{clay-CDB} all these values were positive (1.03–1.62), indicating a relative accumulation of Ce in the iron (hydr)oxides also reported by Pédrot *et al.* (2015); in FF_{clay-Ox} the range was wider (0.86–2.22) and erratic again.

Behaviour of lanthanides in relation to soil horizon evolution and time

The lanthanide concentrations exhibited very different behaviours in the fine sand and clay fractions with regard to the morphological evolution of the soil horizons, measured with the horizon development index (HDI) (Harden, 1982) (Table 4). Positive linear correlations with $P < 0.01$ were typical of the clay fraction, whereas

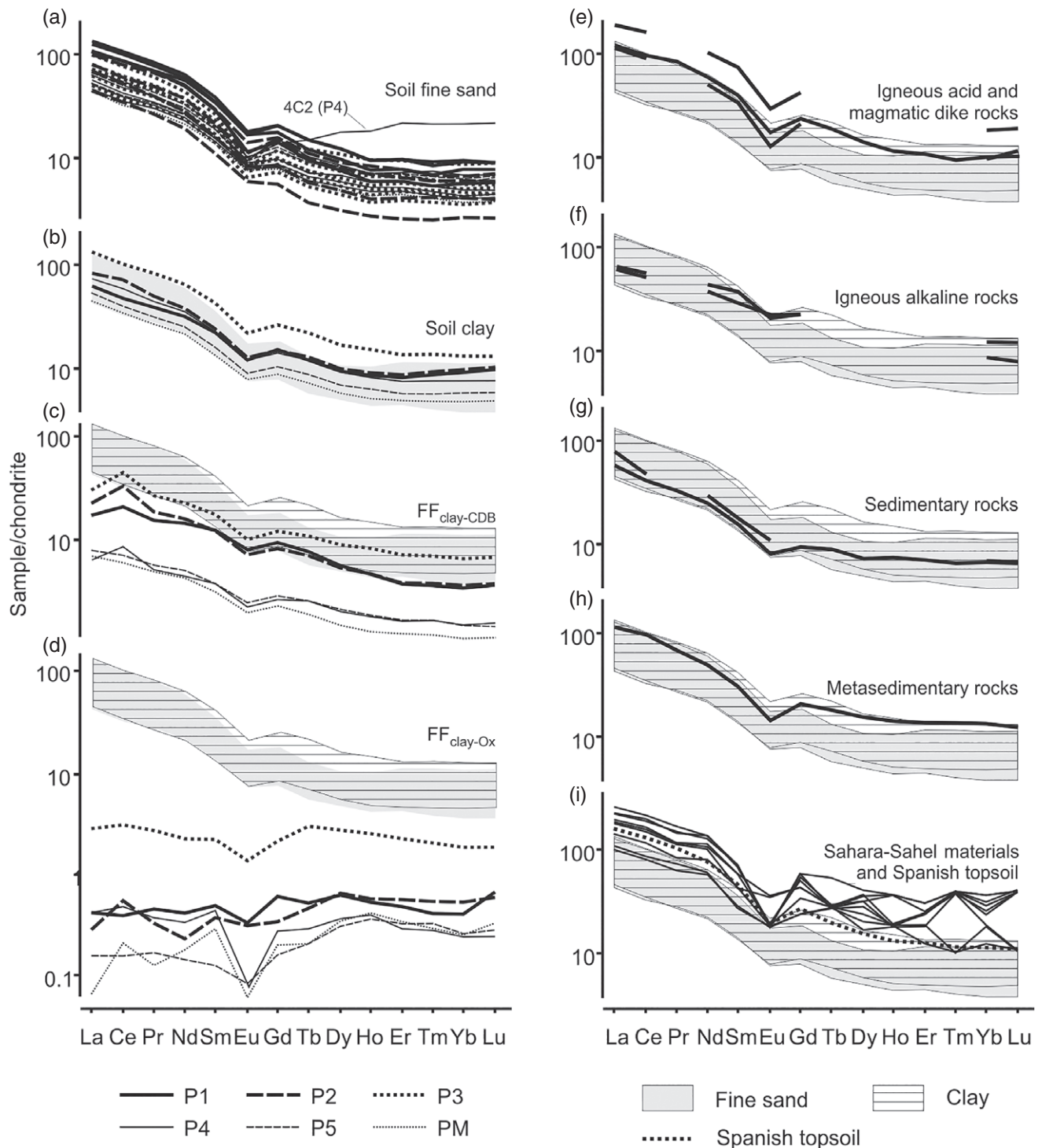


Figure 2 Chondrite-normalized concentrations of lanthanides (logarithmic scale) in: (a) the soil fine sand fraction (50–250 μm) (all horizons; this study), (b) the soil clay fraction (<2 μm) (mean profile, this study), (c) free forms from the soil clay fraction (mean profile, this study) extracted with citrate-dithionite-bicarbonate (FF_{clay-CDB}), (d) free forms from the soil clay fraction (mean profile, this study) extracted with oxalate (FF_{clay-Ox}), (e) acid igneous and magmatic-like rocks from the Guadalquivir catchment (Larrea *et al.*, 1992, 1994, 1995; Carracedo *et al.*, 1997; Pascual *et al.*, 2008), (f) alkaline igneous rocks from the Guadalquivir catchment (Larrea *et al.*, 1995; Pin *et al.*, 2002), (g) sedimentary rocks from the Guadalquivir catchment (Martínez-Ruiz, 1994; Jiménez-Espinoza *et al.*, 2016), (h) metasedimentary rocks from the Guadalquivir catchment (Torres-Ruiz *et al.*, 2003) and (i) Sahara-Sahel materials (Moreno *et al.*, 2006) and Spanish topsoil (Locutura *et al.*, 2012). The shaded area (b to i) and the area with horizontal lines (c to i) enclose the upper and lower margins of the mean values per profile of the fine sand and clays (a and b).

Table 4 Matrix of linear correlations (Pearson's r) between lanthanides content and horizon development index (HDI)^a

Lanthanide content	Soil fine sand ^b ($n = 24$)	Soil clay ^a ($n = 35$)	FF _{clay-CDB} ^a ($n = 35$)	FF _{clay-Ox} ^a ($n = 35$)
La	0.314	0.557	0.718	0.367
Ce	0.317	0.579	0.765	0.483
Pr	0.297	0.565	0.745	0.442
Nd	0.257	0.551	0.746	0.409
Sm	0.192	0.572	0.766	0.503
Eu	0.031	0.526	0.745	0.467
Gd	0.020	0.567	0.741	0.516
Tb	-0.077	0.564	0.746	0.454
Dy	-0.203	0.589	0.745	0.527
Ho	-0.227	0.594	0.740	0.373
Er	-0.267	0.614	0.730	0.403
Tm	-0.227	0.656	0.724	0.431
Yb	-0.213	0.705	0.746	0.484
Lu	-0.219	0.727	0.741	0.517
ΣLn	0.252	0.575	0.762	0.537
ΣLREE	0.304	0.569	0.761	0.461
ΣMREE	0.007	0.571	0.753	0.519
ΣHREE	-0.240	0.656	0.739	0.454

Statistical significance: $P < 0.05$; $P < 0.01$; $P < 0.001$.

^aHDI and lanthanides values from Martín-García *et al.* (2016).

^bLanthanides values from Table 2.

FF_{clay-CDB}, citrate-dithionite-bicarbonate extractable free forms in clay fraction; FF_{clay-Ox}, ammonium oxalate extractable free forms in clay fraction.

there was no significant correlation with the fine sand. Thus, lanthanide concentration in clay increases with horizon evolution, particularly in HREE, which are those with the strongest correlations ($P < 0.001$; $r = 0.656, 0.705, 0.727$ and 0.656 for Tm, Yb, Lu and ΣHREE, respectively). The clay free forms FF_{clay-CDB} showed the same behaviour as the clay fraction, with the correlations being even more significant (with $P < 0.001$), possibly because of the previously mentioned role of iron (hydr)oxides (goethite and haematite, principal constituents of the FF_{clay-CDB}) as scavengers of the lanthanides liberated during alteration of the soil minerals. The ratio Ce/ΣLn (Pédrot *et al.*, 2015) in FF_{clay-CDB} was correlated ($P < 0.05$) with HDI ($r = 0.416$; $n = 35$), suggesting the relative enrichment of Ce in FF_{clay-CDB} in the most morphologically evolved horizons.

Evidence has already been provided to illustrate the dependence of the lanthanides in the present study (properties ΣLn, ΣLREE, ΣHREE, Ce/Ce*, MREE_N/LREE_N and HREE_N/LREE_N) on age groups of soils: pre-Holocene (P1, P2 and P3) and Holocene (P4, P5 and PM). To quantify these relations better, we calculated the correlation matrix of lanthanide concentration with soil age (Table 5). The behaviour was different: the fine sand showed a linear relation with time ($y = ax + b$) and a quadratic relation with time ($y = ax^2 + bx + c$) in LREE and part of MREE (La to Gd), and ΣLn, whereas the clay fraction was fitted well by logarithmic functions ($y = a \ln x + b$) in HREE and another part of MREE (Tb to Lu) and ΣHREE. For the fine sand, this suggests that the concentrations of

lanthanides from La to Gd did not attain a stable state (identified by the logarithmic model). On the other hand, the concentrations in clay of lanthanides from Tb to Lu did attain a stable state. Furthermore, the chronofunctions with strong correlations spanned from La to Gd in fine sand and were present from Gd (not included) in the clay, suggesting the 'gadolinium breaking effect' (Chi *et al.*, 2006). The latter is the infringement of the monotonic change of properties of lanthanide compounds according to the atomic number, attributed to a variation in the electron configuration of the lanthanides occurring in the gadolinium.

When the problem of soil age is considered from the point of view of LREE and HREE fractionation, estimated by the indices HREE_N/LREE_N and La_N/Yb_N (Table 5), it can appear that this process depends markedly on age, with the HREE concentration increasing with time, for example in soil clay:

$$\text{La}_N/\text{Yb}_N = -5.2 \times 10^{-3} \times \text{age (ka)} + 10.39;$$

$$n = 6; R^2 = 0.870; P < 0.01.$$

However, a stable state was not attained for either fine sand or clay because the correlations never fitted the logarithmic functions.

Relations between lanthanide quantities

Although concentrations of elements of the lanthanide series were different in all the fractions analysed (Tables 2 and 3, Figure 2a–d), many changed in a parallel way in the samples showing a strong positive collinearity (large r_{CLC} ; where r_{CLC} are the correlation coefficients between 'couples of lanthanide concentrations') (Figure 3). In the fine sand, the r_{CLC} varied between 0.998 ($P < 0.001$) and 0.477 ($P < 0.001$). In the clay fractions (total clay, FF_{clay-CDB} and FF_{clay-Ox}) r_{CLC} was even larger, ranging from 0.998 to 0.896 (both with $P < 0.001$). Salminen (2005) stated that in European soils 'all REE in soil are strongly correlated among themselves, with all correlation coefficients higher than 0.7'. However, in the present study, more than a third of the r_{CLC} of the fine sand were below 0.7.

Furthermore, r_{CLC} had (Figure 3) the largest values between couples of adjacent lanthanides in the periodic table (e.g. ⁶⁰Nd vs. ⁶¹Pr: 0.998 in fine sand, > 0.945 in clay, FF_{clay-CDB} or FF_{clay-Ox}). This fact was previously reported for igneous materials (Kerr & Rafuse, 2012) and shales (Noack *et al.*, 2015), but never demonstrated for soil.

In addition, r_{CLC} became progressively weaker with increasing separation between the elements in the periodic table (e.g. in fine sand, r_{CLC} of ⁵⁷La with the adjacent ⁵⁸Ce was 0.997, with ⁶⁶Dy, 0.622 and with ⁷¹Lu, at the other extreme, 0.524). This behaviour has never been described previously in geologic materials, and is related to chemical periodicity (adjacent Ln have similar ionic radii, atomic mass and a +3 valence, and will behave similarly in the crystal structure of the minerals). This behaviour of r_{CLC} enables a bivariate diagram to be produced (Figure 4) showing the r_{CLC} of any couple of lanthanides against their differences in standard atomic weight (ΔA_r), with a negative collinearity ($P < 0.001$). The A_r (expressed in decimals) was used because it differentiates more

(a)

	La	Ce	Pr	Nd	Sm	Eu	Gd	Tb	Dy	Ho	Er	Tm	Yb	Lu	
La	1.000														La
Ce	0.997	1.000													Ce
Pr	0.996	0.996	1.000												Pr
Nd	0.991	0.992	0.998	1.000											Nd
Sm	0.976	0.976	0.989	0.995	1.000										Sm
Eu	0.832	0.835	0.848	0.870	0.885	1.000									Eu
Gd	0.891	0.893	0.912	0.928	0.952	0.904	1.000								Gd
Tb	0.770	0.774	0.792	0.812	0.846	0.814	0.960	1.000							Tb
Dy	0.622	0.627	0.646	0.671	0.716	0.719	0.883	0.975	1.000						Dy
Ho	0.513	0.518	0.537	0.562	0.611	0.613	0.804	0.933	0.984	1.000					Ho
Er	0.477	0.481	0.500	0.525	0.577	0.574	0.775	0.913	0.976	0.992	1.000				Er
Tm	0.498	0.503	0.514	0.535	0.579	0.560	0.767	0.907	0.967	0.984	0.992	1.000			Tm
Yb	0.539	0.546	0.555	0.577	0.617	0.621	0.795	0.923	0.972	0.976	0.983	0.986	1.000		Yb
Lu	0.524	0.530	0.542	0.564	0.605	0.605	0.788	0.918	0.969	0.978	0.982	0.982	0.993	1.000	Lu

(b)

	La	Ce	Pr	Nd	Sm	Eu	Gd	Tb	Dy	Ho	Er	Tm	Yb	Lu	
La	1.000														La
Ce	0.989	1.000													Ce
Pr	0.997	0.986	1.000												Pr
Nd	0.994	0.978	0.998	1.000											Nd
Sm	0.978	0.959	0.988	0.994	1.000										Sm
Eu	0.963	0.937	0.975	0.983	0.994	1.000									Eu
Gd	0.958	0.930	0.972	0.981	0.995	0.992	1.000								Gd
Tb	0.962	0.938	0.976	0.984	0.996	0.993	0.998	1.000							Tb
Dy	0.962	0.939	0.976	0.983	0.995	0.989	0.997	0.998	1.000						Dy
Ho	0.964	0.942	0.977	0.983	0.995	0.990	0.995	0.997	0.998	1.000					Ho
Er	0.959	0.942	0.973	0.978	0.992	0.986	0.992	0.994	0.995	0.996	1.000				Er
Tm	0.948	0.936	0.961	0.965	0.981	0.974	0.981	0.983	0.986	0.987	0.995	1.000			Tm
Yb	0.927	0.920	0.942	0.944	0.964	0.954	0.963	0.965	0.969	0.973	0.984	0.992	1.000		Yb
Lu	0.896	0.896	0.914	0.917	0.942	0.933	0.945	0.946	0.951	0.955	0.970	0.983	0.994	1.000	Lu






(c)

	La	Ce	Pr	Nd	Sm	Eu	Gd	Tb	Dy	Ho	Er	Tm	Yb	Lu	
La	1.000														La
Ce	0.949	1.000													Ce
Pr	0.992	0.961	1.000												Pr
Nd	0.986	0.957	0.997	1.000											Nd
Sm	0.969	0.960	0.989	0.994	1.000										Sm
Eu	0.959	0.947	0.981	0.990	0.996	1.000									Eu
Gd	0.955	0.951	0.977	0.986	0.994	0.996	1.000								Gd
Tb	0.957	0.964	0.977	0.984	0.992	0.992	0.996	1.000							Tb
Dy	0.956	0.968	0.972	0.976	0.984	0.980	0.989	0.995	1.000						Dy
Ho	0.954	0.967	0.965	0.970	0.976	0.971	0.981	0.988	0.996	1.000					Ho
Er	0.946	0.959	0.952	0.956	0.962	0.955	0.966	0.975	0.988	0.996	1.000				Er
Tm	0.941	0.955	0.947	0.950	0.955	0.948	0.958	0.968	0.983	0.993	0.997	1.000			Tm
Yb	0.941	0.965	0.948	0.949	0.958	0.948	0.960	0.971	0.987	0.993	0.996	0.996	1.000		Yb
Lu	0.927	0.960	0.937	0.942	0.954	0.947	0.956	0.971	0.981	0.985	0.987	0.986	0.991	1.000	Lu

(d)

	La	Ce	Pr	Nd	Sm	Eu	Gd	Tb	Dy	Ho	Er	Tm	Yb	Lu	
La	1.000														La
Ce	0.780	1.000													Ce
Pr	0.914	0.915	1.000												Pr
Nd	0.882	0.859	0.945	1.000											Nd
Sm	0.789	0.799	0.815	0.761	1.000										Sm
Eu	0.637	0.690	0.760	0.678	0.719	1.000									Eu
Gd	0.776	0.896	0.908	0.911	0.784	0.784	1.000								Gd
Tb	0.750	0.886	0.846	0.793	0.809	0.752	0.909	1.000							Tb
Dy	0.715	0.817	0.835	0.779	0.708	0.837	0.911	0.983	1.000						Dy
Ho	0.770	0.822	0.858	0.995	0.768	0.855	0.898	0.912	0.957	1.000					Ho
Er	0.682	0.757	0.736	0.677	0.697	0.802	0.835	0.905	0.913	0.957	1.000				Er
Tm	0.673	0.782	0.775	0.707	0.708	0.859	0.824	0.938	0.901	0.918	0.903	1.000			Tm
Yb	0.673	0.748	0.768	0.687	0.731	0.858	0.799	0.949	0.884	0.899	0.898	0.879	1.000		Yb
Lu	0.671	0.690	0.732	0.707	0.675	0.776	0.843	0.925	0.870	0.874	0.873	0.806	0.811	1.000	Lu

for (a) and (d):

-  $r_{cl,c} > 0.850$ ($P < 0.001$)
-  $0.850 > r_{cl,c} > 0.750$ ($P < 0.001$)
-  $0.750 > r_{cl,c} > 0.629$ ($P < 0.001$)
-  $0.629 > r_{cl,c} > 0.515$ ($P < 0.01$)
-  $0.515 > r_{cl,c}$ ($P > 0.01$)

for (b) and (c):






-  $r_{cl,c} > 0.990$
 -  $0.990 > r_{cl,c} > 0.970$
 -  $0.970 > r_{cl,c} > 0.940$
 -  $0.940 > r_{cl,c} > 0.900$
 -  $0.900 > r_{cl,c} > 0.890$
- $P < 0.001$

Figure 3 Matrix of Pearson correlation coefficients of couples of lanthanide concentrations (r_{CLC}) in the Mediterranean soils studied: (a) the soil fine sand fraction (50–250 μm), (b) the soil clay fraction (<2 μm), (c) free forms extracted from the soil clay fraction with citrate-dithionite-bicarbonate extract (FF_{clay-CDB}) and (d) free forms extracted from the soil clay fraction with oxalate (FF_{clay-Ox}).

Table 5 Correlation (R^2 , coefficient of determination) between lanthanide contents and geochemical ratio with soil age ($n = 6$). Selected chronofunctions (s).

Lanthanide properties	Soil fine sand ^{a,b}			Soil clay ^{a,c}			FF _{clay-CDB} ^{a,c}			FF _{clay-Ox} ^{a,c}		
	Linear	Logarithmic		Linear	Logarithmic		Linear	Logarithmic		Linear	Logarithmic	
		(ln)	Quadratic		(ln)	Quadratic		(ln)	Quadratic			
La	0.794(s)	0.643	0.824	0.005	0.469	0.241	0.211	0.526	0.429	0.032	0.338	0.049
Ce	0.801(s)	0.616	0.841	0.004	0.486	0.391	0.106	0.494	0.524	0.000	0.234	0.102
Pr	0.785(s)	0.593	0.835	0.011	0.496	0.229	0.183	0.501	0.381	0.033	0.309	0.046
Nd	0.787(s)	0.555	0.854	0.014	0.506	0.194	0.215	0.523	0.389	0.040	0.278	0.046
Sm	0.752(s)	0.494	0.859	0.058	0.607	0.192	0.251	0.563	0.410	0.064	0.276	0.077
Eu	0.823(s)	0.323	0.945	0.083	0.624	0.188	0.324	0.593	0.444	0.227	0.436	0.324
Gd	0.613	0.416	0.796	0.092	0.645	0.168	0.329	0.588	0.440	0.138	0.358	0.147
Tb	0.365	0.389	0.578	0.086	0.664	0.208	0.241	0.554	0.378	0.052	0.279	0.111
Dy	0.127	0.237	0.372	0.102	0.676	0.224	0.195	0.546	0.364	0.032	0.275	0.150
Ho	0.016	0.155	0.176	0.099	0.674	0.230	0.171	0.520	0.326	0.005	0.184	0.067
Er	0.001	0.094	0.189	0.153	0.743	0.300	0.130	0.490	0.298	0.023	0.250	0.115
Tm	0.000	0.100	0.134	0.207	0.764	0.365	0.122	0.471	0.314	0.012	0.164	0.020
Yb	0.025	0.154	0.181	0.314	0.865	0.493	0.126	0.491	0.329	0.006	0.219	0.129
Lu	0.010	0.144	0.142	0.411	0.893	0.500	0.163	0.510	0.364	0.043	0.308	0.222
ΣLn	0.762(s)	0.596	0.819	0.013	0.523	0.285	0.165	0.526	0.446	0.020	0.277	0.078
ΣLREE	0.796(s)	0.608	0.841	0.006	0.493	0.301	0.150	0.516	0.464	0.009	0.269	0.060
ΣMREE	0.582	0.438	0.760	0.080	0.638	0.191	0.265	0.570	0.407	0.072	0.315	0.124
ΣHREE	0.010	0.126	0.176	0.222	0.805	0.386	0.136	0.496	0.317	0.013	0.228	0.108
HREE _N /LREE _N	0.324	0.070	0.462	0.752	0.068	0.906	0.293	0.255	0.830	0.082	0.551	0.083
La _N /Yb _N	0.533	0.412	0.870	0.850	0.171	0.865	0.300	0.003	0.325	0.027	0.226	0.108

s: Selected linear chronofunction^c from fine sand fraction:

$$\text{La (mg kg}^{-1}\text{)} = 0.022 \times \text{age (ka)} + 14.17$$

$$\text{Ce (mg kg}^{-1}\text{)} = 0.050 \times \text{age (ka)} + 27.75$$

$$\text{Pr (mg kg}^{-1}\text{)} = 0.006 \times \text{age (ka)} + 3.46$$

$$\text{Nd (mg kg}^{-1}\text{)} = 0.021 \times \text{age (ka)} + 12.80$$

$$\text{Sm (mg kg}^{-1}\text{)} = 0.004 \times \text{age (ka)} + 2.52$$

$$\text{Eu (mg kg}^{-1}\text{)} = 0.001 \times \text{age (ka)} + 0.47$$

$$\Sigma\text{Ln (mg kg}^{-1}\text{)} = 0.107 \times \text{age (ka)} + 68.15$$

$$\Sigma\text{LREE (mg kg}^{-1}\text{)} = 0.099 \times \text{age (ka)} + 58.19$$

Statistical significance: $P < 0.05$; $P < 0.01$.

^aSoil age values from Table 1.

^bLanthanide values from Table 2.

^cLanthanide values from Table 3 and Martín-García *et al.* (2016).

FF_{clay-CDB}, citrate-dithionite-bicarbonate extractable free forms in clay fraction; FF_{clay-Ox}, ammonium oxalate extractable free forms in clay fraction.

precisely between couples than Z (expressed in units) and is more independent of valency than effective ionic radii (IR). However, A_r , Z and IR are equivalent magnitudes, with strong collinearity (Table 6).

The equation of the straight line ΔA_r against r_{CLC} shows different values from its slope (m), depending on the granulometric fraction: (i) fine sand, $m = -0.0170$ and (ii) clay, -0.0021 , FF_{clay-CDB} -0.0015 and FF_{clay-Ox} -0.0051 . Thus, m becomes a granulometric differentiating characteristic.

In Figure 4(c) (FF_{clay-CDB}), the behaviour of Ce is interesting because it shows slightly stronger correlation with the elements furthest from A_r (Ce against Tb to Lu: $0.955 < r_{\text{CLC}} < 0.968$; mean = 0.963; $\sigma_{n-1} = 0.005$) than with those nearest (Ce against La to Gd: $0.947 < r_{\text{CLC}} < 0.960$; mean = 0.954; $\sigma_{n-1} = 0.006$), and is thus related better to the HREE than LREE. This is because of

FF_{clay-CDB} being free from forms of iron (goethite and haematite) where the process of oxidative scavenging of Ce takes place: part of the Ce³⁺ adsorbed on to Fe (hydr)oxides oxidizes to Ce⁴⁺, producing a preferential desorption of the remaining Ce³⁺ (Bau, 1999; Pédrot *et al.*, 2015), and the Ce⁴⁺ accumulated in the FF_{clay-CDB} behaves similarly to the HREE (Pédrot *et al.*, 2015). Further evidence for this is the preferential fractionation of Ce and HREE in FF_{clay-CDB} described in the samples. Furthermore, Figure 3(c) shows a change in tendency of the r_{CLC} values in the correlations between Ce and Gd (0.951) and Ce and Tb (0.964), once again suggesting the gadolinium breaking effect (Chi *et al.*, 2006).

Evidence for fractionation and fingerprints of provenance

The La – 5 × Sm – 10 × Yb triangle (Figure 5) shows the population of the fine sand and clay plotted close together as a cluster

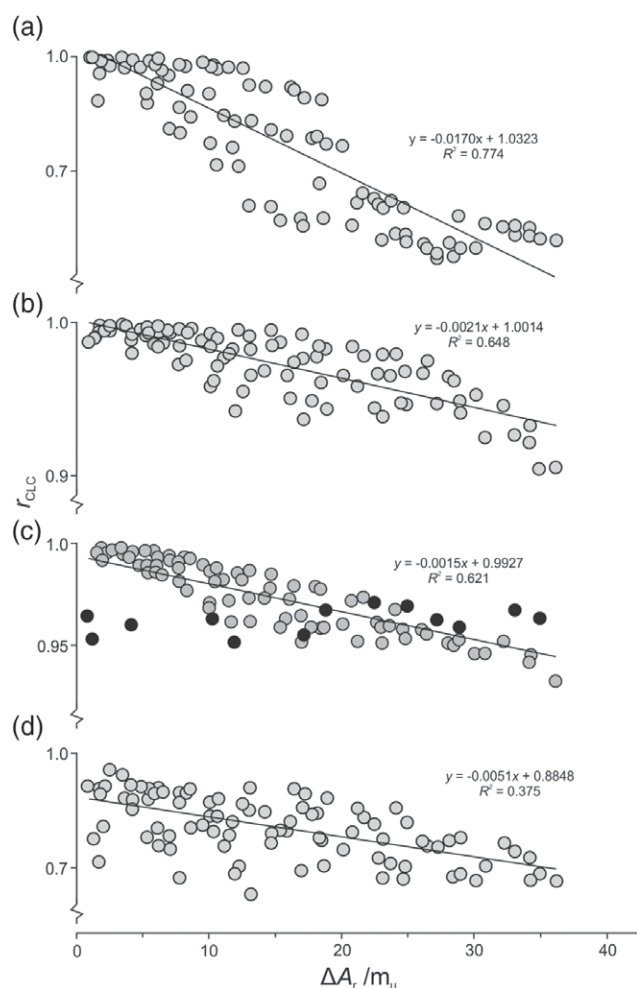


Figure 4 Relations between differences in atomic weight (ΔA_r) and Pearson correlation coefficients of couples of lanthanide concentrations (r_{CLC}) in: (a) the soil fine sand fraction (50–250 μm), (b) the soil clay fraction (< 2 μm), and (c) free forms extracted from the soil clay fraction with citrate-dithionite-bicarbonate ($\text{FF}_{\text{clay-CDB}}$). The black circles represent correlations with Ce and (d) free forms extracted from the soil clay fraction with oxalate ($\text{FF}_{\text{clay-Ox}}$). In all cases: $n = 91$; $P < 0.001$.

(except for the fine sand of 4C2 of P4). As La represents the LREE, Sm the MREE and Yb the HREE, the fractionation of LREE and of HREE in fine sand compared with clay is demonstrated by proximity of the points of the former to the vertex of La and the points of the latter to $10 \times \text{Yb}$. Figure 5 also shows that the cluster of samples includes the parent rocks of soils such as acidic igneous rocks, quaternary sediments and carbonate and metamorphic rocks, slightly separated from the alkaline igneous rocks. Initial interpretation could be that: (i) fine sand and clay are related genetically and (ii) the lanthanides in the soil originate from these parent rocks and could potentially be used as fingerprints of provenance. The point for the Spanish soils is close to the cluster; the Sahara–Sahel materials are also close, even coinciding with our clays.

Table 6 Chemical and physical properties of lanthanides

Name	Chemical symbol	Atomic number (Z) ^a	A_r/m_u ^{a,b}	Valency ^c	Effective ionic radii (IR)/pm ^{a,c}
Lanthanum	La	57	138.9	3	116.0
Cerium	Ce	58	140.1	3, 4	114.3
Praseodymium	Pr	59	140.9	3	112.6
Neodymium	Nd	60	144.2	3	110.9
Promethium ^d	Pm	61	–	3	–
Samarium	Sm	62	150.4	2, 3	107.9
Europium	Eu	63	152.0	2, 3	106.6
Gadolinium	Gd	64	157.3	3	105.3
Terbium	Tb	65	158.9	3, 4	104.0
Dysprosium	Dy	66	162.5	3	102.7
Holmium	Ho	67	164.9	3	101.5
Erbium	Er	68	167.3	3	100.4
Thulium	Tm	69	168.9	3	99.4
Ytterbium	Yb	70	173.1	2, 3	98.5
Lutetium	Lu	71	175.0	3	97.7

^aThere is strong collinearity between A_r and Z and IR: $Z = 0.3640 \cdot A_r + 7.1654$, $r = 0.997$; $\text{IR} = -0.4787 \cdot A_r + 180.6$, $r = 0.991$ ($n = 14$, $P < 0.001$). In the case of IR, the equivalence is a result of the periodic rule known as ‘lanthanide contraction’.

^b A_r is the standard atomic weight (Meija *et al.*, 2016).

^cValency and effective ionic radii for VIII Ln^{+3} (Shannon, 1976).

^dPm has no stable isotopes.

The chondrite-normalized profiles of lanthanide concentration (Figure 2) also appear to show the genetic relation ‘fine-sand with clay’ and ‘fine-sand + clay with parent rock’. Fine sand and clay (Figure 2a,b) have profiles that are close together and the profiles of igneous (Figure 2e,f), sedimentary (Figure 2g) and metasedimentary (Figure 2h) rocks are included in the shaded area representing our samples.

Similarly, mean values of fine sand and clay of $\Sigma(\text{La, Ce, Nd, Sm, Eu, Yb, Lu})$ (only these seven Ln were analysed in all the studies on the geological materials of the Guadalquivir basin) (Figure 6) are within the mean values of the rocks of the Guadalquivir catchment area, although closer in value to those of the sedimentary and alkaline igneous rocks than to the others. The ratio of La_N/Yb_N (Figure 6) further emphasizes this tendency; the values for our samples form a cluster with a range of 7.2–15.7, within the range of the geological materials of the source area (range 3.3–20.4). The fine sand (range 9.8–15.7) had larger values than the clays (range 7.2–11.0) and would be closer to acidic igneous than sedimentary rocks. Notwithstanding this difference between fine sand and clay, it seems more likely that the fractionation of the lanthanides, rather than different source areas for the two fractions, resulted in the fine sand having a larger concentration of La than Yb. The $\Sigma(\text{La, Ce, Nd, Sm, Eu, Yb, Lu})$ (Figure 6) also shows that our samples have smaller values than the Sahara–Sahel materials or even the Spanish soils (both possible aeolian source areas). In contrast, La_N/Yb_N values do not explain the differences between our samples and the Sahara–Sahel materials or the Spanish soils as they are all between 6.9 and 14.3 (except clay of P1 and fine sand of P2, which are close).

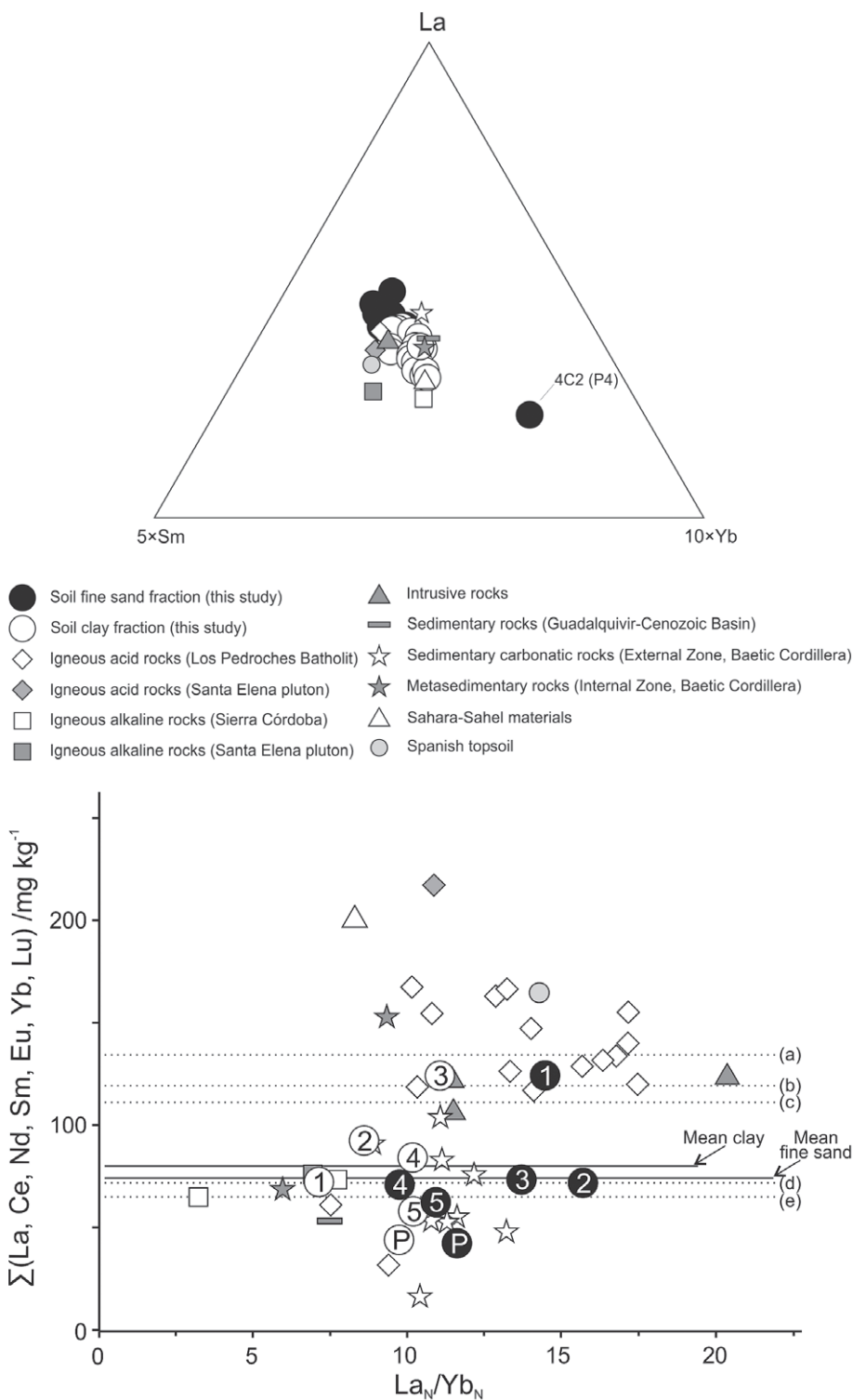


Figure 5 Triangular diagram of La–5Sm–10Yb for soil fine sand and clay fractions (all samples) and mean values of parent rocks of soils from the Guadalquivir catchment (igneous, sedimentary and metasedimentary rocks; Larrea *et al.*, 1992, 1994, 1995; Martínez-Ruiz, 1994; Carracedo *et al.*, 1997; Pin *et al.*, 2002; Pascual *et al.*, 2008; Jiménez-Espinoza *et al.*, 2016), Sahara–Sahel materials (Moreno *et al.*, 2006) and Spanish topsoil (Locutura *et al.*, 2012).

Figure 6 Plot of La_N/Yb_N against Σ(La, Ce, Nd, Sm, Eu, Yb, Lu) for soil fine sand and soil clay fractions (mean profile values) and all values for rocks from the Guadalquivir catchment (igneous, sedimentary and metasedimentary rocks; Larrea *et al.*, 1992, 1994, 1995; Martínez-Ruiz, 1994; Carracedo *et al.*, 1997; Pin *et al.*, 2002; Pascual *et al.*, 2008; Jiménez-Espinoza *et al.*, 2016), Sahara–Sahel materials (Moreno *et al.*, 2006) and Spanish topsoil (Locutura *et al.*, 2012). Symbols used are the same as in Figure 5; the numbers in the circles correspond to soil profile number and P to point bar sediment (PM). The horizontal lines within the figure correspond to the mean values of Σ(La,Ce,Nd,Sm,Eu,Yb,Lu) from: (a) acid igneous rocks (135 mg kg⁻¹), (b) intrusive rocks (119 mg kg⁻¹), (c) metasedimentary rocks (112 mg kg⁻¹), (d) alkaline igneous rocks (72 mg kg⁻¹) and (e) sedimentary carbonatic rocks (65 mg kg⁻¹); soil clay fraction 80 mg kg⁻¹ and soil fine sand fraction 75 mg kg⁻¹.

The ratio of Sm_N/Yb_N functions in a similar way to La_N/Yb_N (Figure 7). The fine sand had larger values than the clay. When La_N/Yb_N was plotted against Sm_N/Yb_N the points were aligned as expected because they have a common denominator, and La and Sm correlate well with each other (Figure 3). However, three families

of points can be defined to which linear functions fitted well: (i) igneous rocks, (ii) sedimentary and metamorphic rocks (metasedimentary) and (iii) our fine sand and clay samples. The linear functions fitted to these families of points suggest a lithological relation. Furthermore, the family of points for fine

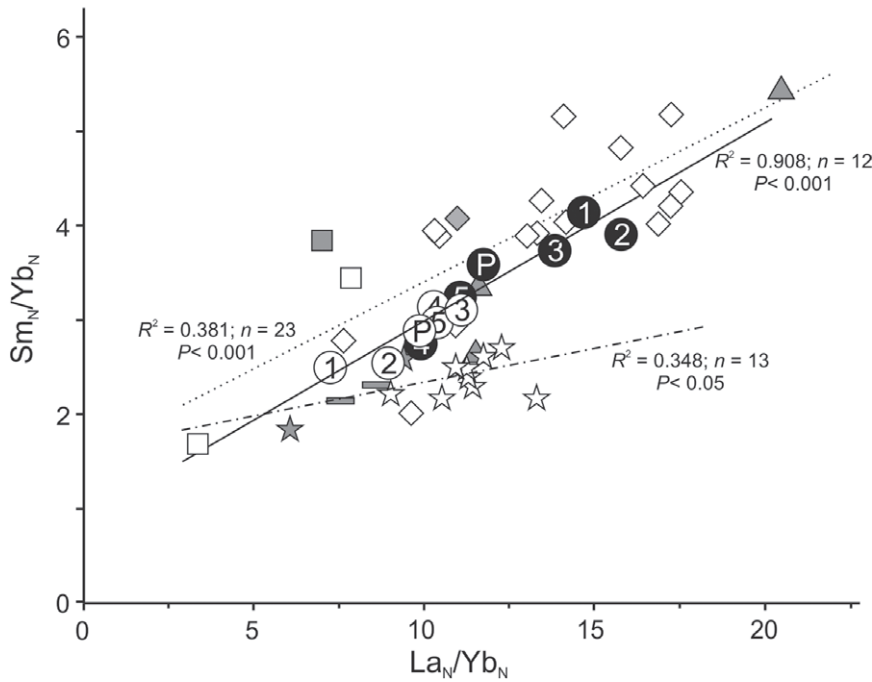


Figure 7 Plot of La_N/Yb_N against Sm_N/Yb_N for soil fine sand and clay fractions (mean profile values) and all values for rocks from the Guadalquivir catchment (igneous, sedimentary and metasedimentary rocks; Larrea *et al.*, 1992, 1994, 1995; Martínez-Ruiz, 1994; Carracedo *et al.*, 1997; Pin *et al.*, 2002; Pascual *et al.*, 2008; Jiménez-Espinosa *et al.*, 2016). Symbols used are the same as in Figure 5; the numbers in the circles correspond to soil profile numbers, and P corresponds to point bar sediment (PM). The lines (and adjacent equations) correspond to the relations for the population of samples of fine sand and clay fractions (continuous), the igneous rocks (dots) and the sedimentary and metasedimentary rocks (dots and dashes).

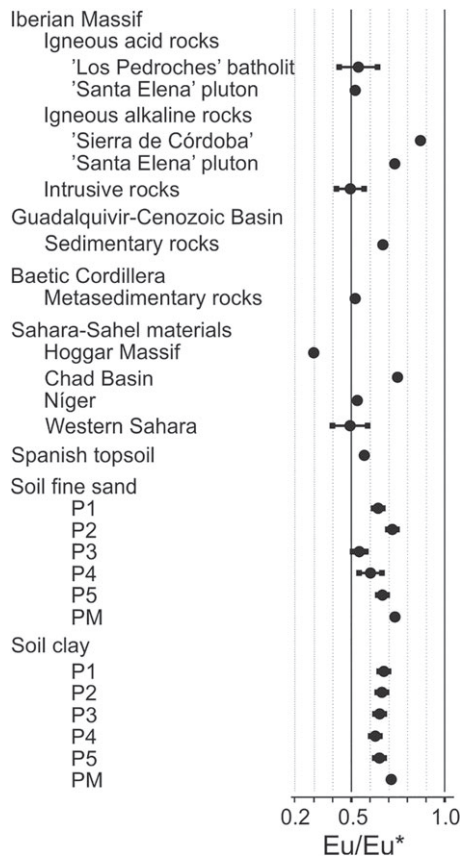


Figure 8 The Eu/Eu^* values (mean and, in some cases, standard deviation) for soil fine sand and clay fractions (mean profile) and rocks from the Guadalquivir catchment (igneous, sedimentary and metasedimentary rocks), Sahara–Sahel materials and Spanish topsoil.

sand and clay is between the lines of the igneous and sedimentary + metamorphic rocks, indicating that both materials could act as parent materials. However, in this case, in contrast to $\Sigma(La, Ce, Nd, Sm, Eu, Yb, Lu)$, the straight line is closer to the igneous rocks, including its slope value.

The Eu/Eu^* anomaly had similar values for fine sand and clay (Table 3, Figure 8); in fact, the correlation between $Eu/Eu^*_{\text{fine sand}}$ and Eu/Eu^*_{clay} was positive and significant ($r = 0.560$; $n = 24$; $P < 0.01$). Furthermore, the anomaly was always negative (< 1), a characteristic shared with the materials from the possible source areas (including aeolian) (Figure 8). The relative homogeneity of values between our soil and parent rocks (Figure 8) indicated that this geochemical ratio can be inherited from the sediment source and the weathering processes do not seem to have changed it (Mongelli *et al.*, 2014).

So far, we have not confirmed a genetic relation between our soil and the aeolian contributions from the Sahara–Sahel or Spanish soils (Figure 6). We focus now on the surface horizons (Ap) of our soils and the point bar sediment (PM), which, because they occupy the upper levels of the profile, are more likely to receive these contributions (Figure 9). Our samples form a group, although differentiated between fine sand and clay because of fractionation of the lanthanides (between LREE, concentrated in fine sand, and HREE, relatively concentrated in soil clay). Outside the group, the Sahara–Sahel materials occur at the lower edge of Figure 9 because these are richer in Yb and the genetic relation cannot be confirmed. However, the spot for Spanish soils was included in the cluster of our soil material because surrounding Spanish soils could have provided materials to the Guadalquivir catchment. Nevertheless, the problem is complex because in the Ap the lanthanide concentration

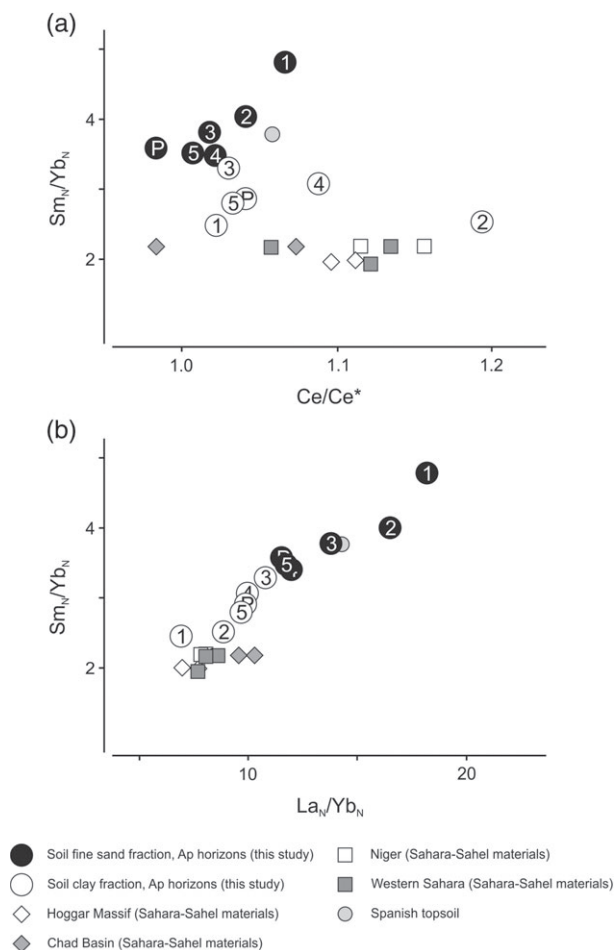


Figure 9 Plot of (a) Ce/Ce^* against Sm_N/Yb_N and (b) La_N/Yb_N versus Sm_N/Yb_N for soil fine sand and clay fractions from Ap horizons (the numbers in the circles correspond to soil profile numbers) and PM (the letter P in the circle corresponds to point bar sediment PM) and Sahara-Sahel materials (Moreno *et al.*, 2006), and Spanish topsoil (Locutura *et al.*, 2012).

of fine sand decreased (Table 2), whereas it increased in clay (Martín-García *et al.*, 2016).

Conclusions

The free forms of clay ($FF_{clay-CDB}$ and $FF_{clay-Ox}$) showed a relative accumulation of lanthanides, with values $> 700 \text{ mg kg}^{-1}$ (with respect to the mass of free form), thus demonstrating their role as scavengers of lanthanides.

Soil age (pre-Holocene versus Holocene) affects the behaviour of the lanthanides in all the fractions studied: in the fine sand $\Sigma LREE$ concentration increased in the oldest soil, as did $\Sigma HREE$ in the clay and its free forms. Furthermore, chronofunctions were formulated between lanthanide concentration and soil age from La to Gd in fine sand and from Tb to Lu in clay. These chronofunction results tended to support the granulometric fractionation cited, and, indirectly, provided data to confirm the presence of a ‘gadolinium breaking effect’.

The concentrations between couples of lanthanides showed strong collinearity, particularly in the clay and its free forms ($FF_{clay-CDB}$ and $FF_{clay-Ox}$), but only partly in the fine sand. This enabled the identification of a new relation, depending on their position in the periodic table, that is valid for all the fractions analysed. For example, the coefficient r_{CLC} decreased significantly with increasing separation between the lanthanide elements in the periodic table, estimated by ΔA_r .

The use of lanthanides as fingerprints of provenance using a variety of properties and geochemical indices ($La-Sm-Yb$, $\Sigma(La, Ce, Nd, Sm, Eu, Yb, Lu)$, La_N/Yb_N , Sm_N/Yb_N , Eu/Eu^* , Ce/Ce^*) suggested a genetic relation between all of them, although it has not been possible to determine the relative contribution of the different materials to our soils. For example, for $\Sigma(La, Ce, Nd, Sm, Eu, Yb, Lu)$ the greatest contribution appeared to be sedimentary rocks, whereas for La_N/Yb_N versus Sm_N/Yb_N it would be igneous rocks.

The Ce fractionates in these soils were concentrated in the clay fraction and its free forms (especially in $FF_{clay-CDB}$, where Ce/Ce^* is > 1) through oxidative scavenging in the iron (hydr)oxides. It behaves more like the heavy lanthanides (HREE) than the light lanthanides (LREE) to which it belongs; it had larger values of r_{CLC} from Gd and Tb, which we attributed to the ‘gadolinium breaking effect’. However, Eu was shown to be inherited from the materials of the Guadalquivir catchment.

Acknowledgements

Sample preparation and chemical analysis were conducted by Emma Humphreys-Williams and Stanislav Strekopytov (Imaging and Analysis Centre, Natural History Museum, London, UK). This work was supported by a grant from Ministerio de Economía, Industria y Competitividad de España (‘Tipologías de Suelos Mediterráneos versus Cuarzo. En la frontera del conocimiento edafogénico’; Ref. CGL2016-80308-P). The authors thank Professor Margaret A. Oliver, an anonymous editor and two anonymous reviewers for helpful comments and suggestions that improved the final manuscript. We also thank Robert Abrahams (Bsc) for revising the English language.

References

- Aide, M. & Smith-Aide, C. 2003. Assessing soil genesis by rare-earth elemental analysis. *Soil Science Society of America Journal*, **67**, 1470–1476.
- Bau, M. 1999. Scavenging of dissolved yttrium and rare earths by precipitating iron oxyhydroxide: experimental evidence for Ce oxidation, Y-Ho fractionation, and lanthanide tetrad effect. *Geochimica et Cosmochimica Acta*, **63**, 67–77.
- Blundy, J. & Wood, B. 2003. Partitioning of trace elements between crystals and melts. *Earth and Planetary Science Letters*, **210**, 383–397.
- British Geological Survey (BGS) 2011. *Rare Earth Elements* [WWW document]. URL <https://www.bgs.ac.uk/downloads/start.cfm?id=1638> [accessed on 10 July 2018].
- Calero, J., Delgado, R., Delgado, G. & Martín-García, J.M. 2008. Transformation of categorical field soil morphological properties into numerical properties for the study of chronosequences. *Geoderma*, **145**, 278–287.

- Calero, J., Delgado, R., Delgado, G. & Martín-García, J.M. 2009. SEM image analysis in the study of a soil chronosequence on fluvial terraces of the middle Guadalquivir (southern Spain). *European Journal of Soil Science*, **60**, 465–480.
- Calero, J., Martín-García, J.M., Delgado, G., Aranda, V. & Delgado, R. 2013. A nano-scale study in a soil chronosequence from southern Spain. *European Journal of Soil Science*, **64**, 192–209.
- Carracedo, M., Larrea, F.J., Alonso-Olazabal, A. & Gil-Ibarguchi, J.I. 1997. The relationship between the plutonic intrusions and the dyke swarm in the Los Pedroches batholith (Iberian Massif, Spain): dykes as a paleotectonic and paleostress indicators. *Cadernos do Laboratorio Xeolóxico de Laxe*, **22**, 229–246.
- Chang, C., Li, F., Liu, C., Gao, J., Tong, H. & Chen, M. 2016. Fractionation characteristics of rare earth elements (REEs) linked with secondary Fe, Mn, and Al minerals in soils. *Acta Geochimica*, **35**, 329–339.
- Chen, L.M., Zhang, G.L. & Jin, Z.D. 2014. Rare earth elements of a 1000-year paddy soil chronosequence: implications for sediment provenances. Parent material uniformity and pedological changes. *Geoderma*, **230**, 274–279.
- Chi, R.A., Dai, Z.X., Xu, Z.G., Wu, Y.X. & Wang, C.W. 2006. Correlation analysis on partition of rare earth in ion-exchangeable phase form weathered crust ores. *Transactions of Nonferrous Metals Society of China*, **16**, 1421–1425.
- Delgado, R., Martín-García, J.M., Oyonarte, C. & Delgado, G. 2003. Genesis of the terrae rossae of the Sierra Gádor (Andalusia, Spain). *European Journal of Soil Science*, **54**, 1–16.
- Gregory, T., Joy, K.H., Strekopytov, S. & Curran, N.M. 2017. Geochemistry and petrology of howardite Miller Range 11100: a lithologically diverse piece of the Vestan regolith. *Meteoritics & Planetary Science*, **52**, 206–224.
- Guastoni, A., Nestola, F., Ferraris, C. & Parodi, G. 2012. Xenotime-(Y) and Sn-rich thortveitite in miarolitic pegmatites from Baveno, Southern Alps, Italy. *Mineralogical Magazine*, **76**, 761–767.
- Harden, J.W. 1982. A quantitative index of soil development from field descriptions: examples from a chronosequence in central California. *Geoderma*, **28**, 1–28.
- Hu, Z., Haneklaus, S., Sparovek, G. & Schnug, E. 2006. Rare earth elements in soils. *Communications in Soil Science and Plant Analysis*, **37**, 1381–1420.
- Huang, C. & Gong, Z. 2001. Geochemical implication of rare earth elements in process of soil development. *Journal of Rare Earths*, **19**, 57–62.
- Jiménez-Espinosa, R., Jiménez-Millán, J. & García-Tortosa, F.J. 2016. Upper-Pleistocene terrace deposits in Mediterranean climate: geomorphological and source-rock control on mineral and geochemical signatures (Betic Cordillera, SE Spain). *Journal of Iberian Geology*, **42**, 187–200.
- Kerr, A. & Rafuse, H. 2012. *Rare-earth Element (REE) Geochemistry of the Strange Lake Deposits: Implications for Resource Estimation and Metallogenic Models*. Report No 12-1. Newfoundland and Labrador Department of Natural Resources, Geological Survey Branch, St. John's, Canada.
- Larrea, F.J., Carracedo, M., Cueto, L.A., Quesada, C., Gil-Ibarguchi, J.I., Fernández, F.J. *et al.* 1992. Petrology and geochemistry of Cardeña-Virgen de La Cabeza pluton (batholith of Los Pedroches). *Cadernos do Laboratorio Xeolóxico de Laxe*, **17**, 209–222.
- Larrea, F.J., Carracedo, M., Ortega, L.A. & Gil-Ibarguchi, J.I. 1994. The Linares granite (Jaén): cartography, petrology and geochemistry. *Cadernos do Laboratorio Xeolóxico de Laxe*, **19**, 335–346.
- Larrea, F.J., Carracedo, M., Ortega, L.A. & Gil-Ibarguchi, J.I. 1995. The Santa Elena stock (Jaén). An intrusion genetically independent from the magmatic association of the Los Pedroches Batholith. *Cadernos do Laboratorio Xeolóxico de Laxe*, **20**, 151–166.
- Laveuf, C. & Cornu, S. 2009. A review on the potentiality of rare earth elements to trace pedogenetic processes. *Geoderma*, **154**, 1–12.
- Laveuf, C., Cornu, S., Guilherme, L.R.G. & Juillot, F. 2012. The impact of redox conditions on the rare earth element signature of redoximorphic features in a soil sequence developed from limestone. *Geoderma*, **170**, 25–38.
- Locutura, J., Bel-lan, A., García-Cortés, A. & Martínez-Romero, S. 2012. *Atlas Geoquímico de España*. IGME, Madrid.
- Marques, R., Prudencio, M.I., Dias, M.I. & Rocha, F. 2011. Patterns of rare earth and other trace elements in different size fractions of clays of Campanian–Maastrichtian deposits from the Portuguese western margin (Aveiro and Taveiro Formations). *Chemie der Erde*, **71**, 337–347.
- Martínez-Ruiz, F. 1994. *Geoquímica y mineralogía del tránsito Cretácico-Terciario en las Cordilleras Béticas y en la Cuenca Vasco-Cantábrica*. Doctoral dissertation, Universidad de Granada, Granada.
- Martín-García, J.M., Sánchez-Marañón, M., Calero, J., Aranda, V., Delgado, G. & Delgado, R. 2016. Iron oxides and rare earth elements in the clay fractions of a soil chronosequence in southern Spain. *European Journal of Soil Science*, **67**, 749–762.
- McDonough, W.F. & Sun, S. 1995. The composition of the Earth. *Chemical Geology*, **120**, 223–253.
- Meija, J., Coplen, T.B., Berglund, M., Brand, W.A., De Bièvre, P., Groning, M. *et al.* 2016. Atomic weights of the elements 2013 (IUPAC Technical Report). *Pure and Applied Chemistry*, **88**, 265–291.
- Mongelli, G., Paternoster, M., Rizzo, G. & Sinisi, R. 2014. Trace elements and REE fractionation in subsoils developed on sedimentary and volcanic rocks: case study of the Mt. Vulture area, southern Italy. *International Journal of Earth Sciences*, **103**, 1125–1140.
- Moreno, T., Querol, X., Castillo, S., Alastuey, A., Cuevas, E., Herrmann, L. *et al.* 2006. Geochemical variations in aeolian mineral particles from the Sahara-Sahel Dust Corridor. *Chemosphere*, **65**, 261–270.
- Noack, C.W., Jain, J.C., Stegmeier, J., Hakala, J.A. & Karamalidis, A.K. 2015. Rare earth element geochemistry of outcrop and core samples from the Marcellus Shale. *Geochemical Transactions*, **16**, 6. <https://doi.org/10.1186/s12932-015-0022-4>.
- Och, L.M., Müller, B., Wichser, A., Ulrich, A., Vologina, E.G. & Sturm, M. 2014. Rare earth elements in the sediments of Lake Baikal. *Chemical Geology*, **376**, 61–75.
- Onac, B.P., Pedersen, R.B. & Tysseland, M. 1997. Presence of rare-earth elements in black ferromanganese coatings from Vântului Cave (Romania). *Journal of Cave and Karst Studies*, **59**, 128–131.
- Pascual, E., Donaire, T. & Pin, C. 2008. The significance of microgranular enclaves in assessing the magmatic evolution of a high-level composite batholith: a case on the Los Pedroches Batholith, Iberian Massif, Spain. *Geochemical Journal*, **42**, 177–198.
- Pédrot, M., Dia, A., Davranche, M. & Gruau, G. 2015. Upper soil horizons control the rare earth element patterns in shallow groundwater. *Geoderma*, **239–240**, 84–96.
- Pin, C., Liñán, E., Pascual, E., Donaire, T. & Valenzuela, A. 2002. Late Neoproterozoic crustal growth in the European Variscides: Nd isotope and geochemical evidence from the Sierra de Córdoba Andesites (Ossa-Morena Zone, Southern Spain). *Tectonophysics*, **352**, 133–151.
- Rollinson, H.R. 1993. *Using Geochemical Data: Evaluation, Presentation, Interpretation*. Prentice Hall, Harlow.

- Salminen, R. (Ed.) 2005. *Geochemical Atlas of Europe. Part 1: Background Information, Methodology and Maps*. IUGS/IAGC. [WWW document]. URL <http://weppi.gtk.fi/publ/foregsatlas/index.php> [accessed on 10 July 2018].
- Shannon, R.D. 1976. Revised effective ionic radii and systematic studies in interatomic distances in halides and chalcogenides. *Acta Crystallographica*, **A32**, 751–767.
- Torres-Ruiz, J., Pesquera, A., Gil-Crespo, P.P. & Velilla, N. 2003. Origin and petrogenetic implication of tourmaline-rich rocks in the Sierra Nevada (Betic Cordillera, southeastern Spain). *Chemical Geology*, **197**, 55–86.
- Wang, G., Li, J., Ravi, S., Van Pelt, R.S., Costa, P.J.M. & Dukes, D. 2017. Tracer techniques in aeolian research: approaches, applications, and challenges. *Earth-Science Reviews*, **170**, 1–16.
- Wen, X.Y., Huang, C.M., Tang, Y., Gong-Bo, S.L., Hu, X.X. & Wang, Z.W. 2014. Rare earth elements: a potential proxy for identifying the lacustrine sediment source and soil erosion intensity in karst areas. *Journal of Soils and Sediments*, **14**, 1693–1702.